Combined Metabolic and Chemical (CoMetChem) labeling using stable isotopes – A strategy to reveal site-specific histone acetylation and deacetylation rates by LC-MS

van Pijkeren A [1, 2#], Dietze J [3#], Sánchez Brotons A [2#], Lijster T [2], Barcaru A [2], Egger AS[1], Hotze M[1], Dekker FJ [4], Horvatovich P [2], Melgert B [5, 6], Ziegler M [7], Thedieck K [1, 8, 9*], Heiland I [3, 10*], Bischoff R [2*], Kwiatkowski M [1,5,6*]

[1] Department of Biochemistry and Center for Molecular Biosciences Innsbruck, University of Innsbruck, Innsbruck, Austria

[2] Department of Analytical Biochemistry and Interfaculty Mass Spectrometry Center, Groningen Research Institute of Pharmacy, University of Groningen, Groningen, the Netherlands

[3] Department of Arctic and Marine Biology, UiT The Arctic University of Norway, Tromsø, Norway

[4] Chemical and Pharmaceutical Biology, Groningen Research Institute of Pharmacy, University of Groningen, Groningen, the Netherlands

[5] Department of Molecular Pharmacology, Groningen Research Institute for Pharmacy, University of Groningen, Groningen, the Netherlands

[6] Groningen Research Institute for Asthma and COPD, University Medical Center Groningen, University of Groningen, Groningen, the Netherlands.

[7] Department of Biomedicine, University of Bergen, Bergen, Norway

[8] Laboratory of Pediatrics, Section Systems Medicine of Metabolism and Signaling, University of Groningen, University Medical Center Groningen, Groningen, the Netherlands.

[9] Department for Neuroscience, School of Medicine and Health Sciences, Carl von Ossietzky University Oldenburg, Oldenburg, Germany.

[10] Neuro-SysMed, Department of Neurology, Haukeland University Hospital, Bergen, Norway, Department of Clinical Medicine, University of Bergen, Bergen, Norway

[#] These authors contributed equally

* These authors contributed equally

Correspondence: marcel.kwiatkowski@uibk.ac.at; r.p.h.bischoff@rug.nl; ines.heiland@uit.no; kathrin.thedieck@uibk.ac.at

Abstract

Histone acetylation is an important, reversible post-translational protein modification and a hallmark of epigenetic regulation. However, little is known about the dynamics of this process, due to the lack of analytical methods that can capture site-specific acetylation and deacetylation reactions. We present a new approach that combines metabolic and chemical labeling (CoMetChem) using uniformly ^{13}C-labeled glucose and stable isotope labeled acetic anhydride. Thereby, chemically equivalent, fully acetylated histone species are generated enabling accurate relative quantification of site-specific lysine acetylation dynamics in tryptic peptides using high-resolution mass spectrometry. We show that CoMetChem enables site-specific quantification of the incorporation or loss of lysine acetylation over time, allowing the determination of reaction rates for acetylation and deacetylation. Thus, the CoMetChem methodology provides a comprehensive description of site-specific acetylation dynamics.

Introduction

Living organisms are highly dynamic systems, constantly exposed to external changes and strive to maintain homeostasis. Posttranslational modifications (PTMs) play a crucial role in this process as they allow to adapt protein function and activity in a rapid and highly dynamic manner. Histone lysine acetylation is a dynamic and reversible PTM regulated by histone acetyltransferases (HATs, also known as lysine acetyltransferases (KATs)) and histone deacetylases (HDACs, also known as lysine deacetylases (KDACs)) [1]. HATs regulate the transfer of a acetyl groups from acetyl-coenzyme A (acetyl-CoA) to ε-amino groups of lysine residues, and HDACs catalyze the removal of acetyl groups

from modified lysines. Histone acetylations are hallmarks of epigenetic regulation and are closely linked to the regulation of key cellular processes such as chromatin remodelling, transcriptional regulation, gene silencing, cell cycle progression, apoptosis, differentiation, DNA replication, DNA repair and nuclear import [1-2]. An imbalance in histone acetylation has been associated with a variety of human diseases including cancer [3], chronic inflammation [4] as well as neurological [5] and metabolic disorders [6].

Despite their central biological and medical importance, the dynamics and site-specificity of acetylation events at histones are still poorly understood. Adjacent PTMs are generally accepted to influence one another [7], but the mechanisms and dynamics by which they control each other's stability and turnover are largely unknown. An important reason for this gap in our knowledge is the lack of adequate methods for the site-specific analysis of acetylation dynamics and their interactions.

Histone modifications are still frequently detected by immunochemical techniques. However, site-specific antibodies against acetyllysines often lack specificity and cross-react with adjacent PTMs in the N-terminal histone tails [8]. Moreover, while they allow to estimate the relative extent of a PTM under different conditions, immunochemical methods cannot be used to trace the turnover of PTMs. Mass spectrometry (MS) coupled to liquid chromatography (LC-MS) has emerged as a powerful method to investigate site-specific histone acetylation [9] providing reliable, site-specific identification and quantification of histone acetyllysine residues. MS-based methods also allow to detect and quantify simultaneously occurring modifications within the same protein sequence in a single experiment. Nevertheless, quantitative analysis of histone acetylation is particularly challenging since the N-terminal histone tails are highly enriched in lysine and arginine residues in a short stretch of amino acids. Trypsin, the protease of choice for histone analysis by LC-MS, does not cleave at the C-terminal side of acetylated lysines due to charge neutralization. Furthermore, the occurrence of adjacent lysines and arginines may lead to random missed cleavage events, resulting in a variety of short hydrophilic peptides, which are difficult to retain on reversed phase (RP) columns. Thereby, a non-homogeneous pool of peptide species is formed in which the same acetylated residue can be present in different peptides. These chemically non-equivalent species render the accurate quantification of distinct acetylated histone species difficult due to their different retention times and ionization efficiencies [10]. To generate a more homogenous pool of acetylated peptides and to increase the retention of hydrophilic peptides during RP chromatography, primary amino groups of extracted histones can be chemically propionylated or acetylated at the protein level prior to tryptic digestion [11]. The chemical acetylation of unmodified lysines, using stable isotope-labeled acetylating reagents allows to quantify abundance levels of acetylated and non-acetylated histone species [12] while retaining site-specific information [13].

These approaches allow us to detect the state of modification at specific residues, but they provide only a static snapshot of histone acetylation levels. They do not allow us to monitor site-specific acetylation dynamics, which is critical to follow the regulation, turnover, and interplay of histone modifications. Stable isotope labeled metabolic precursors can be used to study dynamics of proteins and posttranslational modifications [14]. To study histone acetylation dynamics, Evertts *et al.* [15] and Zheng *et al.* [16] introduced metabolic labeling by uniformly ^{13}C labeled glucose ([U-13C]-Glc) as a metabolic precursor. [U-13C]-Glc is converted into ^{13}C-labelled acetyl-CoA (Figure 1A), which serves as substrate for the acetylation of lysine residues. MS allows us to discriminate between newly ^{13}C-labeled and pre-existing ^{12}C-labeled acetylation sites, which enables determination of histone acetylation half-lifes. However, half-lifes of different acetylated species are not directly comparable. For example, an acetylated histone species whose substrate is 10 times more abundant compared to another one with the same half-life, is turned over ten times faster. Thus, the substrate abundance must be taken into account in order to directly compare the dynamics of different acetylated species. The substrate abundance of the species whose half-lives are to be compared can be determined by mass

spectrometry. However, in order to be comparable, the analytes must have the same ionization efficiency, i.e. the species to be compared must be chemically equivalent, but distinguishable by mass spectrometry. This is not the case for acetylated versus non-acetylated peptides.

To tackle this issue, we developed a combined metabolic and chemical labeling (CoMetChem) approach. CoMetChem combines [U-13C]-Glc-based metabolic labelling and chemical acetylation of non-acetylated lysine residues with [$^{13}C_4$,D_6]-acetic anhydride ([$^{13}C_4$,D_6]-AA) at the protein level prior to LC-MS analysis. Thereby, all lysine residues of the histones are fully acetylated. Consequently, all peptide species generated during proteolytic digest with identical amino acid sequences exhibit the same chemical properties, permitting accurate relative quantification by MS. Based on the mass shifts introduced by metabolic versus chemical labeling, CoMetChem allows to quantify site-specific acetylation and deacetylation rates, a critical parameter to monitor the dynamics of PTMs and the effects of pharmacological modulators such as HDAC inhibitors.

Materials and Methods

The experimental details are described in the Supporting Information.

Results and Discussion

Chemical acetylation

Unmodified lysine residues are chemically acetylated using stable isotope labeled [$^{13}C_4$,D_6]-AA, which generates $^{13}C_2D_3$-containing acetyllysines (Figure 1 A). These acetyl groups have a mass increment of 5.0252 Da and 3.0185 Da compared to those derived from [U-12C]-Glc ($^{12}C_2H_3$) and [U-13C]-Glc ($^{13}C_2H_3$), respectively (Figure 1 A, B). The mass increments can be resolved in state-of-the art TOF and orbitrap mass analyzers, and the different isotopologues have the same electrospray ionization efficiencies.

Complete chemical acetylation of the non-acetylated lysine residues at the protein level is essential for the CoMetChem strategy to ensure that only chemically equivalent species arise from the tryptic digestion of a given protein. We obtained an almost complete derivatization with both triethylammonium bicarbonate (99.7 ± 1.0%, c= 100 mM, pH 8.5) and sodium borate as a reaction buffer (99.4 ± 1.6 %, c= 100 mM, pH 8.5) (Figure S1 A). The derivatization efficiency was evaluated by LC-MS analysis of 14 histone lysine residues including the H3(18-26) and the H4(4-17) peptides harboring two and four lysine residues, respectively. Acetylating lysine residues that are in close proximity to each other was particularly challenging. While both triethylammonium bicarbonate (99.9 ± 0.2%) and sodium borate (99.8 ± 0.2%) resulted in a near complete acetylation for the H3(18-26) peptide, which contains two lysine residues (Figure S1 B), sodium borate (97.9 ± 0.3%) resulted in a significantly higher acetylation efficiency for the four-lysine containing H4(4-17) peptide compared to triethylammonium bicarbonate (96 ± 0.5 %) (Figure S1 C). Thus, we continued to use sodium borate as a reaction buffer for chemical acetylation with [$^{13}C_4$,D_6]-AA.

Site-specific acetylation turnover

To analyze site-specific acetylation turnover by CoMetChem in cells, we combined metabolic and chemical labeling with [U-13C]-Glc and [$^{13}C_4$,D_6]-AA, respectively. The H3(18-26) peptide species were chosen as an example. The macrophage cell line RAW 264.7 was first cultured in [U-12C]-Glc-containing medium, and then shifted to [U-13C]-Glc-containing medium (t=0) (Figure 1 B). Histones were isolated at different time-points after t=0 over a period of 24 hours and subjected to chemical derivatization with $^{13}C_4$,D_6-AA, trypsin digestion and LC-MS/MS-analysis. The H3 peptide 18-26, generated from the H3 protein by tryptic digestion, covers a region with two adjacent acetylation sites (K18, K23). Thus, combined metabolic and chemical labelling by CoMetChem results in 9 different H3(18-26) peptide isotopologues (Figure 1 C). At the MS1 level, only six of these species could be resolved (Figure 1 D) as the remaining species are isobaric and can only be distinguished based on

their fragment ion spectra (Figure S2). At t=0, before the addition of [U-13C]-Glc, the following isotopologues can be detected (Figure 1 C, D):

I: The non-acetylated H3(18-26) peptide which contains two $^{13}C_4$,D_6-AA derived acetyl groups (m/z 540.8479).

II, III: The endogenously single-acetylated H3(18-26) species, which contain a [U-12C]-Glc derived acetyl group at K18 (II) or K23 (III), and a $^{13}C_4$,D_6-AA derived acetyl group at K23 (II) and K18 (III), respectively (m/z of 538.3353). Both species are isobaric and cannot be distinguished at MS1.

IV: The H(18-26) peptide with two endogenous [U-12C]-Glc derived acetyl groups (m/z 535.8230).

Cultivation in presence of [U-13C]-Glc in combination with chemical acetylation using $^{13}C_4$,D_6-AA led to the formation of the following additional H3(18-26)-isotopologues (Figure 1C, D):

V, VI: The endogenously single-acetylated H3(18-26) species, which contain a [U-13C]-Glc derived acetyl group at K18 (V) or K23 (VI), and a $^{13}C_4$,D_6-AA derived acetyl group at K23 (V) and K18 (VI), respectively (m/z 539.3382). Both species are isobaric and cannot be distinguished at MS1.

VII, VIII: The endogenously double-acetylated H3(18-26) species, which contain a [U-13C]-Glc derived acetyl group at K18 (VII) or K23 (VIII), and a [U-12C]-Glc derived acetyl group at K23 (VII) and K18 (VIII), respectively, which are isobaric at MS1 (m/z 536.8262).

IX: The endogenously double-acetylated H3(18-26) species, which contains two [U-13]-Glc derived acetyl groups (m/z 537.8306).

The single-acetylated species I and II, V and VI, as well as the metabolically double-acetylated species VII and VIII are positional isomers and isobaric at MS1 (Figure 1 D) but are distinguishable based on their fragment ion spectra. In case of the K18ac and K23ac positional isomers derived from [U-13C]-Glc (V, VI), the b3 fragment ions contained either an acetyllysine derived from [U-13C]-Glc for K18 (m/z 414.2593) or a chemically acetylated lysine for K23 (m/z 417.2828) (Figure S2 C). The y7 fragment ions contained either a chemically acetylated lysine for K18 (m/z 777.4940) or an acetyllysine derived from [U-13C]-Glc for K23 (m/z 774. 4755, Figure S2 D). As the fragment ions differ in their stable isotopic composition and their m/z values, the stoichiometry of the K18ac and K23ac species can be determined based on the relative abundance of the respective fragment ions.

Since chemical derivatization leads to chemically equivalent isotopologues, it enables quantification of the relative abundance of the different acetylated H3(18-26) peptides. However, another factor contributes to the complexity of the isotopologue mixture, namely the naturally occurring ^{13}C in the peptide backbone resulting in additional overlapping isotopologues at the MS1 level (Figure 1 D). We therefore included an isotope correction in the data analysis to ensure accurate quantification. The python-based isotope correction pipeline PICor used a skewed matrix algorithm, which corrects each different isotopologue species with its own set of theoretical correction factors (for details see [17]).

Comparison of the relative abundance levels of the different acetylated H3(18-26) species revealed that the endogenously non-acetylated species was the most abundant (50.2%), followed by the single-acetylated K23ac species (30.6%), the double acetylated K18acK23ac species (14.1%) and the single-acetylated K18ac species (5.1%) (Figure 2 A). The levels were stable over the time course of 24 h and across all biological replicates (Figure S3), highlighting the tight control of the acetylation levels at these residues.

To monitor acetylation dynamics, site-specific label incorporation for the single- and double-acetylated species was quantified. We observed a maximum relative label exchange of 40% for all acetylated species (Figure 2B-D). which is comparable to the results reported by Zhen *et al.* [16], where [U-13C]-Glc was used for metabolic labeling without additional chemical acetylation. Individual

turnover rates (k) were calculated by fitting experimental values to exponential growth or decay functions to calculate the site-specific half-lifes ($t_{1/2}$= ln2/k) (Figure 2 E). The single-acetylated species K23ac showed a half-life of 218±26 min, whereas the acetyllysine at K18 showed a half-life of 352±28 min. The double acetylated H3(18-26) peptide (Figure 1 C, IV) can be converted into three different isotopologues (Figure 1C, VII, VIII, IX). Thus, the exponential growth or decay functions used above to determine half-lifes and turnover, can only be used to calculate the total half-life of the double-acetylated peptide (Figure 2 E) and cannot be used to correctly calculate site-specific turnover. The double acetylated species showed a half-life of 236±18 min.

As stated earlier, half-lifes are not directly comparable for substrates with different abundances. Using the CoMetChem approach, generating chemically equivalent species, we were, however, able to calculate the individual acetylation turnover for the single-and double acetylated H3(18-26) species by multiplying the turnover rate (k) with the abundance (A) of the respective peptide species. The single-acetylated K23ac and K18ac-species showed a turnover of 5.8%/h and 0.6%/h (Figure 2F), respectively. Thus, the single-acetylated species had a 10 times faster turnover at K23ac compared to K18ac. The overall turnover of the double acetylated peptide was calculated to be 2.4%/h.

Site-specific reaction rates for acetylation and deacetylation

The calculation of turnover does still represent a simplified description of the acetylation dynamics as it does not provide a comprehensive description of all modification events that occur: each acetylation turnover event involves at least one acetylation and one deacetylation reaction. For example, the nine different H3 species covered by the H3(18-26) peptide are interconverted by at least 12 different reactions (Figure 3 A).

Since CoMetChem enables the direct comparison of the abundance of all peptide species, we were able to determine individual acetylation and deacetylation rates for all H3(18-26) species. However, it is not possible to calculate rates for species that are not present before label addition (dashed arrows in Figure 3). For our calculations, we adapted an approach presented earlier by Zheng et al. [18] for histone methylation analysis. The strategy is based on linear fitting of the initial interconversion fluxes, where the fluxes are the slopes of the time courses (Figure 3B-E) and thus represent the increase or decrease of the different acetylated peptide species over time. This approach is based on the simplified assumption that the substrate concentration is initially relatively constant and, therefore, the corresponding products initially increase linearly with time. To estimate the acetylation and deacetylation rates (υ), the measured fluxes need to be divided by the relative abundance of the respective substrate at t= 0 (see Materials and Methods for details). We determined site-specific acetylation (Figure 3 B, C) and deacetylation rates (Figure 3 D, E) for the single-acetylated peptide. The acetylation rate at K23 (a2, Figure 3 C) was determined to be 0.016±0.002/h whereas deacetylation rate at the same site (d2, Figure 3 E) was 0.058±0.006/h. For K18, we obtained an acetylation rate (a1, Figure 3 B) of 0.004±0.0002/h and a deacetylation rate (d1, Figure 3 D) of 0.031±0.008/h. The comparison of the single-acetylated H3(18-26) species revealed that the acetylation rate for K23 (a2) is approximately four times higher than the acetylation rate at K18 (a1). The difference in site-specific deacetylation rates at K18 (d1) and K23 (d2) is not as pronounced as in the acetylation rates, but K23ac still showed a two-times faster deacetylation rate compared to K18ac. Thus, acetylation and deacetylation rates can substantially differ between lysines within the same peptide.

As we cannot determine which of the [U-12C]-Glc derived single-acetylated species (II or III, Figure 3 A) is produced when the [U-12C]-Glc derived double-acetylated species (IV, Figure 3 A) is deacetylated, it was not possible to deduce the site-specific turnover for double-acetylated species. We can, however, deduce the total deacetylation rate for double-acetylated species (represented by reaction d3 in Figure 3 A). With 0.08/h±0.03 (Figure 3 H), it was approximately equal to the sum of the rates (d1, d2) determined for the site-specific deacetylation rates of the single-acetylated species

(Figure 3 D, E). This indicates that in the H3(18-23)-peptide, the site-specific deacetylation rates were not affected by the acetylation state of the nearby lysine residue.

In contrast to deacetylation rates, the CoMetChem approach allows to determine site-specific acetylation rates for the formation of the double-acetylated peptide. This is based on the conversion of the single-acetylated H3(18-26) species II and III into the double acetylated species VIII and VII by reactions a3 and a4, respectively (Figure 3 A). The site-specific acetylation rates at K18 (a4) and K23 (a3) for the double acetylated species were calculated to be 0.008±0.001/h and 0.043±0.009/h, respectively (Figure 3 F, G). They are thus two to three times faster than for the single-acetylated peptides. This indicates that an already existing acetylation promotes the acetylation of the nearby site in the H3(18-23)-peptide.

We further explored the CoMetChem approach to investigate site-specific acetylation dynamics upon pharmacological intervention with two HDAC inhibitors. We used suberanilohydroxamic acid (SAHA) [19] (Figure S5 A), which inhibits class I, II and IV HDACs, and the benzamide derivative Entinostat (MS-275) [20] (Figure S5 B), which inhibits the class I HDACs HDAC1 and HDAC3. RAW264.7 cells were first cultured in a [U-12C]-Glc containing medium for 22 hours, followed by a pre-incubation of 16 hours with either SAHA or MS-275 (Figure S5 C). Afterwards, the culture medium was replaced by a [U-13C]-Glc containing medium including the corresponding HDAC inhibitor.

As expected, the HDAC inhibitors led to decreased deacetylation. This is reflected in the significant increase of the double acetylated H3(18-26) from 13.3% to 20.4% with MS-275 and to 29.1% with SAHA. In addition, the abundance of the corresponding endogenously non-acetylated H3(18-26) species was reduced from 50% to 38% with MS-275 and to 30% with SAHA (Figure 4 A). The changes in the single acetylated peptides were not as pronounced. Still the abundance of the single acetylated K18ac species was significantly increased upon SAHA, while MS-275 did not alter the abundance of this site. In contrast, the abundance of the single acetylated K23ac species was elevated by MS-275, but not upon SAHA exposure. These results point to differences in site-specificity between HDACs targeted by MS-275 or SAHA, respectively.

Finally, we evaluated the effects of SAHA and MS-275 on the acetylation and deacetylation rates of the H3[18-26] species (Figure 4 B, C). The deacetylation rate for the double-acetylated peptide (d3) was 0.07±0.02/h with MS-275 and thus similar to the control. In contrast, SAHA decreased the deacetylation rate from 0.08±0.03/h to 0.04±0.02/h (Figure 4 D). A comparison of the site-specific deacetylation rates for the single-acetylated H3(18-26) species (d1 and d2) revealed that MS-275 reduced the deacetylation rates at K23(d2) from 0.058±0.006/h to 0.020±0.007/h, and from 0.031±0.008/h to 0.013±0.007/h at K18(d1). With SAHA the acetylation at K18 appeared to be relatively constant, indicating a near complete inhibition of the deacetylation at this site. We note, however, that this requires further investigation as the measured values were at the detection limits of the method. The deacetylation rate at K23 was reduced from 0.058±0.006//h to 0.021±0.007/h upon exposure to SAHA. Treatment with SAHA or MS-275 did not change the acetylation rates at K18 for the single- (a1) or double-acetylated (a4) H3(18-26) species compared to the control (Figure 4 E). Similarly, treatment with SAHA resulted in acetylation rates similar to control at K23 for both the single-acetylated (a2) and double-acetylated species (a3), while treatment with MS-275 resulted in higher acetylation rates at K23 for both the single-acetylated (a2, 0.019±0.001/h) and double-acetylated (a3, 0.065±0.010/h) species compared to the control (single-acetylated K23: 0.016±0.002/h, double-acetylated K23: 0.043±0.009/h). Taken together, we demonstrate that our CoMetChem approach allows us to identify site-specificity of HDACs through the use of HDAC inhibitors.

Conclusion

With the CoMetChem methodology, we present a novel approach for the analysis of site-specific histone acetylation dynamics and reaction rates. The combinatorial use of stable isotope labeled metabolic precursors ([U-13C]-Glc) and chemical acetylation using $^{13}C_4$,D_6-AA results in fully acetylated tryptic peptide isotopologues, which are chemically equivalent. The isotopologues only differ in their mass due to their isotopic composition while having the same ionization and ion transmission efficiencies during MS analysis. Due to the chemical equivalence of the peptide species, site-specific abundance levels can be determined with high precision and site-specific abundance-corrected turnovers can be calculated. These turnovers describe the acetylation dynamics much more accurately than half-lives and allow the kinetics of individual acetylation sites to be directly compared. Thereby, CoMetChem goes beyond half-lives and turnovers, as site-specific acetylation and deacetylation rates can be determined, allowing a comprehensive assessment of the dynamics of this reversible modification, expanding the repertoire of dynamic proteomics methods. This makes CoMetChem a particularly valuable approach to unravel site selectivity of HDACs and protein acetyl transferases and will facilitate the development of HDAC inhibitors with well characterized substrate profiles.

Acknowledgement

M.K. thanks the European Respiratory Society (ERS, RESPIRE3, project reference: R3201703-00121) and the University of Innsbruck (project no: 316826) for financial support. J.D., I.H. and M.Z. have been supported by the Norwegian Research Foundation (ES633272; 302314). K.T., I.H. and M.Z. acknowledge support from the MESI-STRAT project, which has received funding from the European Union Horizon 2020 Research and Innovation Program under the grant agreement no: 754688. A.S.B. and P.H. have received funding from the Netherlands X-omics Initiative, which is partially funded by NWO (project no: 184.034.019). F.J.D. thanks the European Research Council with an ERC starting grant (309782) and Netherlands Organization of Scientific Research (NOW, VIDI grant: 723.012.005) for financial support.

References

[1] T. Narita, B. T. Weinert, C. Choudhary, *Nat Rev Mol Cell Biol* **2019**, *20*, 156-174.
[2] aK. M. Keck, L. F. Pemberton, *Biochim Biophys Acta* **2012**, *1819*, 277-289; bM. Koprinarova, M. Schnekenburger, M. Diederich, *Curr Top Med Chem* **2016**, *16*, 732-744; cS. Peleg, C. Feller, A. G. Ladurner, A. Imhof, *Trends Biochem Sci* **2016**, *41*, 700-711; dC. E. Barnes, D. M. English, S. M. Cowley, *Essays Biochem* **2019**, *63*, 97-107.
[3] J. E. Audia, R. M. Campbell, *Cold Spring Harb Perspect Biol* **2016**, *8*, a019521.
[4] T. van den Bosch, M. Kwiatkowski, R. Bischoff, F. J. Dekker, *Epigenomics* **2017**, *9*, 1013-1028.
[5] S. Shukla, B. L. Tekwani, *Front Pharmacol* **2020**, *11*, 537.
[6] X. Li, C. Li, G. Sun, *J Diabetes Res* **2016**, *2016*, 4065382.
[7] G. Duan, D. Walther, *PLoS Comput Biol* **2015**, *11*, e1004049.
[8] aS. B. Rothbart, S. Lin, L. M. Britton, K. Krajewski, M. C. Keogh, B. A. Garcia, B. D. Strahl, *Sci Rep* **2012**, *2*, 489; bS. B. Rothbart, B. M. Dickson, J. R. Raab, A. T. Grzybowski, K. Krajewski, A. H. Guo, E. K. Shanle, S. Z. Josefowicz, S. M. Fuchs, C. D. Allis, T. R. Magnuson, A. J. Ruthenburg, B. D. Strahl, *Mol Cell* **2015**, *59*, 502-511.
[9] M. C. Volker-Albert, A. Schmidt, I. Forne, A. Imhof, *Curr Protoc Protein Sci* **2018**, *92*, e54.
[10] aK. C. Cho, J. W. Kang, Y. Choi, T. W. Kim, K. P. Kim, *J Mass Spectrom* **2016**, *51*, 105-110; bJ. Hermans, S. Ongay, V. Markov, R. Bischoff, *Anal Chem* **2017**, *89*, 9159-9166.
[11] aC. M. Smith, P. R. Gafken, Z. Zhang, D. E. Gottschling, J. B. Smith, D. L. Smith, *Anal Biochem* **2003**, *316*, 23-33; bT. Bonaldi, A. Imhof, J. T. Regula, *Proteomics* **2004**, *4*, 1382-1396; cB. A. Garcia, S. Mollah, B. M. Ueberheide, S. A. Busby, T. L. Muratore, J. Shabanowitz, D. F. Hunt, *Nat Protoc* **2007**, *2*, 933-938.
[12] T. van den Bosch, N. G. J. Leus, H. Wapenaar, A. Boichenko, J. Hermans, R. Bischoff, H. J. Haisma, F. J. Dekker, *Pulm Pharmacol Ther* **2017**, *44*, 88-95.
[13] D. Vitko, P. Majek, E. Schirghuber, S. Kubicek, K. L. Bennett, *J Proteome Res* **2016**, *15*, 2579-2594.
[14] A. van Pijkeren, R. Bischoff, M. Kwiatkowski, *Analyst* **2019**, *144*, 6812-6833.
[15] A. G. Evertts, B. M. Zee, P. A. Dimaggio, M. Gonzales-Cope, H. A. Coller, B. A. Garcia, *J Biol Chem* **2013**, *288*, 12142-12151.
[16] Y. Zheng, P. M. Thomas, N. L. Kelleher, *Nat Commun* **2013**, *4*, 2203.
[17] J. Dietze, A. v. Pijkeren, M. Kwiatkowski, M. Ziegler, I. Heiland, *bioRxiv* **2020**.
[18] Y. Zheng, S. M. Sweet, R. Popovic, E. Martinez-Garcia, J. D. Tipton, P. M. Thomas, J. D. Licht, N. L. Kelleher, *Proceedings of the National Academy of Sciences of the United States of America* **2012**, *109*, 13549-13554.
[19] P. A. Marks, R. Breslow, *Nat Biotechnol* **2007**, *25*, 84-90.

[20] T. Suzuki, T. Ando, K. Tsuchiya, N. Fukazawa, A. Saito, Y. Mariko, T. Yamashita, O. Nakanishi, *J Med Chem* **1999**, *42*, 3001-3003.

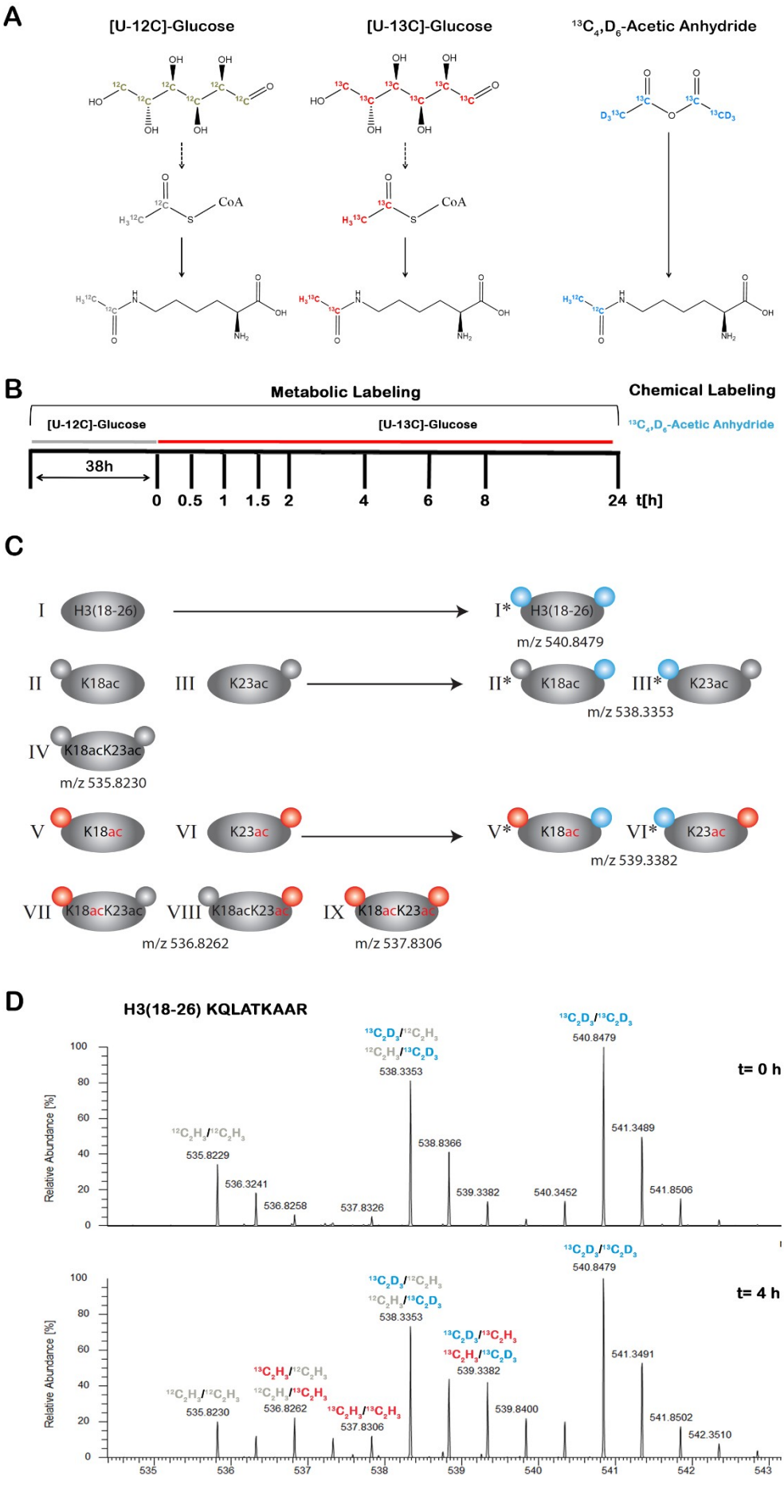
A
[U-12C]-Glucose
[U-13C]-Glucose
13C4,D6-Acetic Anhydride
B
Metabolic Labeling
Chemical Labeling
[U-12C]-Glucose
[U-13C]-Glucose
13C4,D6-Acetic Anhydride
38h
0 0.5 1 1.5 2 4 6 8 24 t[h]
C
I H3(18-26)
I* H3(18-26)
m/z 540.8479
II K18ac
III K23ac
II* K18ac
III* K23ac
m/z 538.3353
IV K18acK23ac
m/z 535.8230
V K18ac
VI K23ac
V* K18ac
VI* K23ac
m/z 539.3382
VII K18acK23ac
VIII K18acK23ac
IX K18acK23ac
m/z 536.8262
m/z 537.8306
D
H3(18-26) KQLATKAAR
t= 0 h
t= 4 h
Relative Abundance [%]

Figure 1: Workflow of the combined metabolic and chemical labeling approach (CoMetChem) for the measurement of site-specific histone acetylation dynamics. (A) The CoMetChem approach combines metabolic and chemical labeling using stable isotopes. The metabolic labeling using [U-12C]-Glucose or [U-13C]-Glucose results in $^{12}C_2H_3$ (grey) or $^{13}C_2H_3$ (red) containing acetyllysine residues. The chemical acetylation of non-acetylated lysines using $^{13}C_6$,D_6-Acetic anhydride results in $^{13}C_2D_3$ (blue) containing acetyllysine residues. (B) To investigate site-specific acetylation dynamics by the CoMetChem approach, RAW264.7 cells were first cultured in a [U-12C]-Glucose containing medium (grey) followed by medium replacement to [U-13C]-Glucose containing medium (red). After cultivation, the nuclei were isolated from the samples at different time points, followed by histone extraction, chemical derivatization of unmodified lysine residues at the protein level using $^{13}C_6$,D_6-Acetic anhydride (blue), tryptic digestion and quantitative LC-MS analysis. (C) Schematic representation of all possible acetylated H3 species covered by the H3(18-26) peptide generated metabolically (left panel, Roman numerals without asterisk) and the corresponding isotopologues generated by combination with chemical acetylation (right panel, Roman numerals with asterisk). Acetyl groups derived from [U-12C]-Glucose are indicated by gray, [U-13C]-Glucose derived acetyl groups are indicated by red, and $^{13}C_6$,D_6-Acetic anhydride derived acetyl groups are indicated by blue circles, and the m/z values of the different isotopologues are shown. (D) MS1 spectrum of the H3(18-26) isotopologues upon combined metabolic and chemical labeling after medium exchange (t= 0) and 4h incubation with [U-13C]-Glucose (t= 4h). The spectra show the different H3(18-26) isotopologues and the colors indicate whether the acetyl groups of the K18 (left) and K23 (right) residues are derived from [U-12C]-Glucose (gray), [U-13C]-Glucose (red) or $^{13}C_6$,D_6-Acetic anhydride (blue).

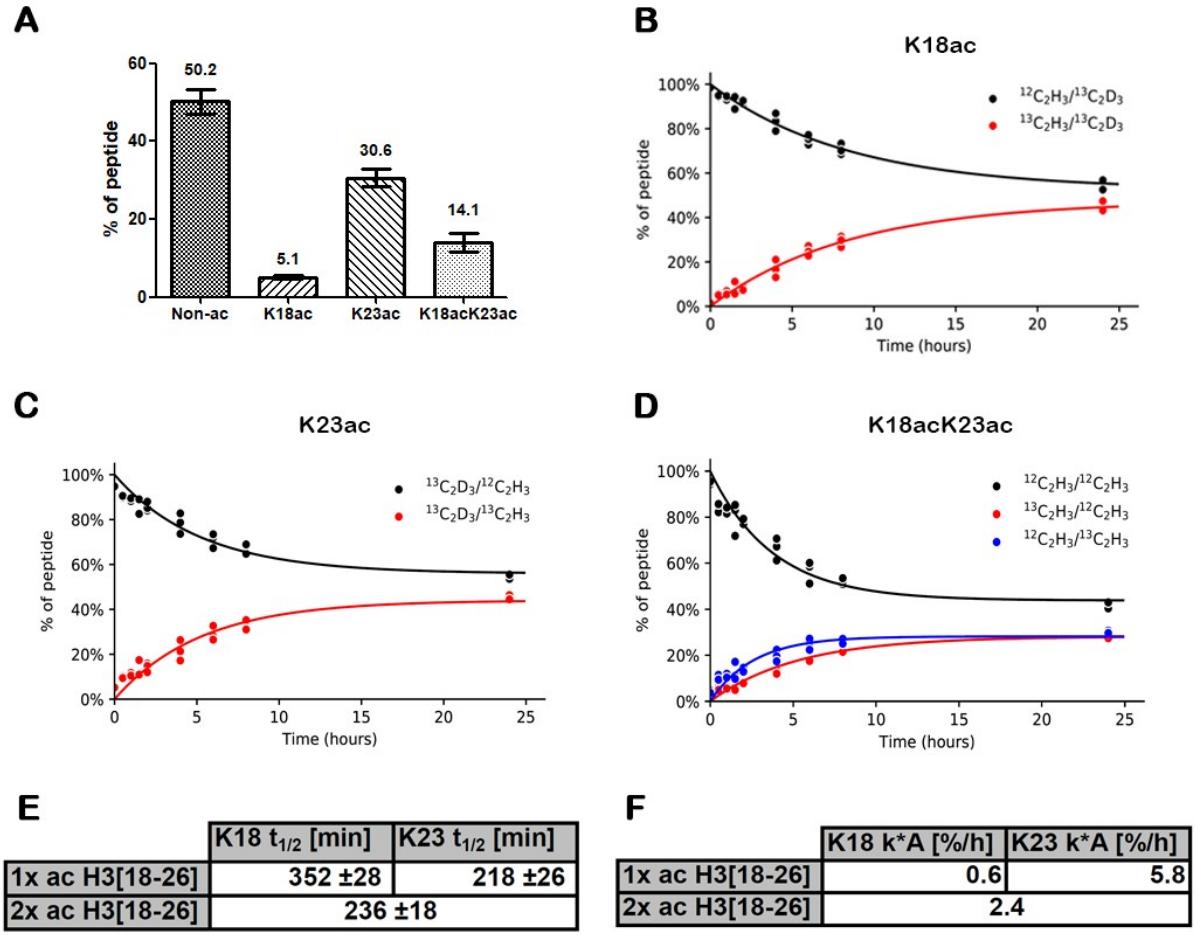

E

	K18 $t_{1/2}$ [min]	K23 $t_{1/2}$ [min]
1x ac H3[18-26]	352 ±28	218 ±26
2x ac H3[18-26]	236 ±18	

F

	K18 k*A [%/h]	K23 k*A [%/h]
1x ac H3[18-26]	0.6	5.8
2x ac H3[18-26]	2.4	

Figure 2: Site-specific abundance levels, half-lifes and turnover of the single- and double-acetylated H3(18-26) peptide species. A: Bar charts (median with standard deviation) showing abundance levels of the non-acetylated (Non-Ac), single-acetylated (K18ac, K23ac) and double-acetylated (K18acK23ac) H3(18-26) species averaged over a time course of 24 hours. B, C: Site-specific label incorporation and label loss of the single-acetylated H3(18-26) species with an acetyllysine at K18ac (B) or K23ac (C). D: Site-specific label incorporation and label loss of K18ac and K23ac of the double-acetylated H3(18-26) species. E: Site-specific half-lifes of K18ac and K23ac of the single-acetylated (1x ac) and half-life of the double-acetylated (2x ac) H3(18-26) species. F: Site-specific turnover of K18ac and K23ac of single-acetylated (1x) ac and turnover of the double-acetylated (2x ac) H3(18-26) species. n = 3 independent experiments.

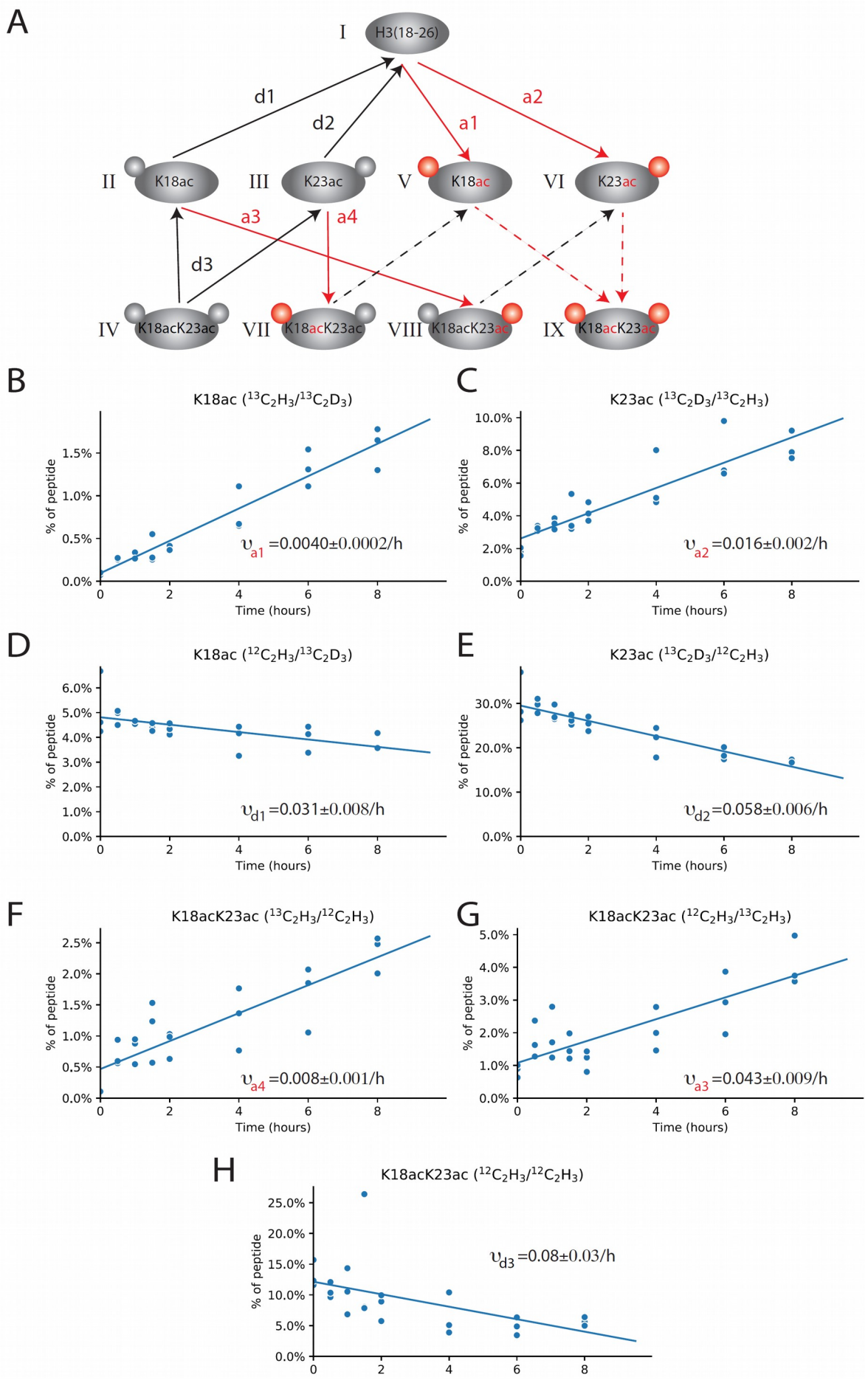
A
I H3(18-26)
d1
d2
a1
a2
II K18ac
III K23ac
V K18ac
VI K23ac
a3
a4
d3
IV K18acK23ac
VII K18acK23ac
VIII K18acK23ac
IX K18acK23ac
B
K18ac ($^{13}C_2H_3/^{13}C_2D_3$)
% of peptide
Time (hours)
υ_{a1} =0.0040±0.0002/h
C
K23ac ($^{13}C_2D_3/^{13}C_2H_3$)
% of peptide
Time (hours)
υ_{a2} =0.016±0.002/h
D
K18ac ($^{12}C_2H_3/^{13}C_2D_3$)
% of peptide
Time (hours)
υ_{d1} =0.031±0.008/h
E
K23ac ($^{13}C_2D_3/^{12}C_2H_3$)
% of peptide
Time (hours)
υ_{d2} =0.058±0.006/h
F
K18acK23ac ($^{13}C_2H_3/^{12}C_2H_3$)
% of peptide
Time (hours)
υ_{a4} =0.008±0.001/h
G
K18acK23ac ($^{12}C_2H_3/^{13}C_2H_3$)
% of peptide
Time (hours)
υ_{a3} =0.043±0.009/h
H
K18acK23ac ($^{12}C_2H_3/^{12}C_2H_3$)
% of peptide
υ_{d3} =0.08±0.03/h

Figure 3: Initial flux analysis to determine acetylation and deacetylation rates: A: schematic representation of possible in vivo generated H3[18-26] species and reactions occurring in the metabolic labeling approach. Red arrows represent acetylation reactions (marked as ‘’a’’) and black arrows represent deacetylation reactions (marked as ‘’d’’). Dashed arrows represent reactions for which initial flux fitting is not possible as the respective labelled substrates are not present at time point t= 0. B-D: Linear fit of the measurements from samples taken within 8 hours after addition of [U-13C]-Glucose used to calculate the acetylation rates of the single-acetylated H3(18-26) species with an acetyllysine at K23ac (B, a1) and K18ac (C, a2), the deacetylation rates at K23ac (D, d1) and K18ac (E, d2), the acetylation rates of the double-acetylated H3(18-26) species with an acetyllysine at K23ac (F, a4) and K18ac (G, a3), and the deacetylation rate (H, d3).

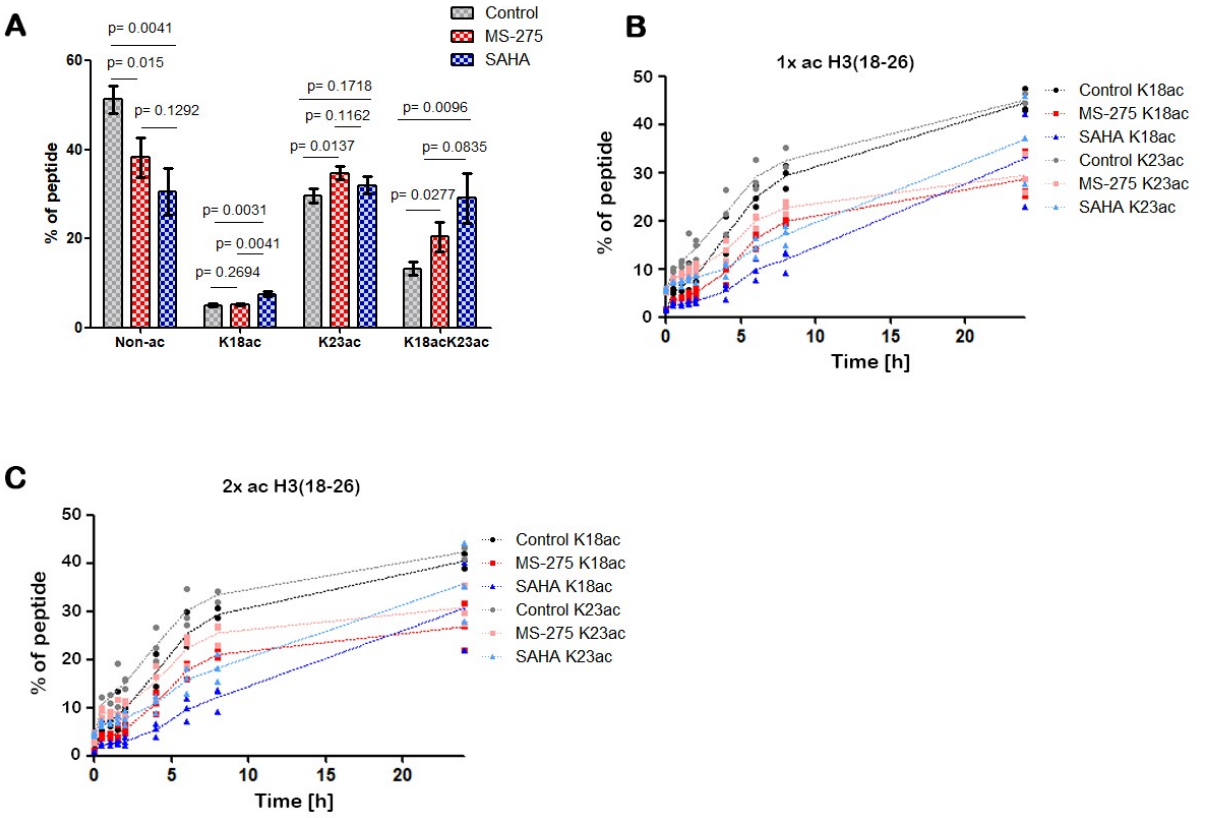

D **Deacetylation rates**

1x ac H3[18-26]	K18 υ [h^{-1}]	K23 υ [h^{-1}]
Control	0.031 ±0.008	0.058 ±0.006
MS-275	0.013 ±0.007	0.020 ±0.007
SAHA	not determined	0.021 ±0.007

2x ac H3[1826]	K18K23 υ [h-1]
Control	0.084 ±0.026
MS-275	0.067 ±0.026
SAHA	0.040 ±0.018

E **Acetylation rates**

1x ac H3[18-26]	K18 υ [h^{-1}]	K23 υ [h^{-1}]
Control	0.004 ±0.0002	0.016 ±0.002
MS-275	0.004 ±0.0002	0.019 ±0.001
SAHA	0.004 ±0.0002	0.014 ±0.001

2x ac H3[18-26]	K18 υ [h^{-1}]	K23 υ [h^{-1}]
Control	0.008 ±0.001	0.043 ±0.009
MS-275	0.010 ±0.001	0.065 ±0.010
SAHA	0.009 ±0.001	0.050 ±0.007

Figure 4: Effect of the histone deacetylase inhibitors MS-275 and SAHA on the site-specific acetylation levels and the acetylation and deacetylation rates of the single-acetylated and double-acetylated H3(18-26) peptide species. A: Bar chart (mean with standard deviation) showing abundance levels of the non-acetylated (Non-Ac), single-acetylated (K18ac, K23ac) and double-acetylated (K18acK23ac) H3(18-26) species after 16 hours of incubation with MS-275 (c= 1 µM, in 0.01% DMSO containing medium), SAHA (c= 0.41 µM, in 0.01% DMSO containing medium) or the carrier (control: 0.01% DMSO containing medium). B, C: Site-specific label incorporation for K18ac and K23ac of the single acetylated H3(18-26) species (B) and the double-acetylated H3(18-26) species (C). Levels of newly incorporated acetyl groups (% of peptide) were determined by dividing the peak areas of the individual acetyllysine-containing peptide species upon [U-13C]-Glucose derived acetylation by the sum of the peak areas upon [U-13C]-Glucose and [U-12C]-Glucose derived acetylation. D: Site-specific deacetylation rates of K18ac and K23ac of the single-acetylated (1x ac) H3(18-26) species, and deacetylation rate for the double-acetylated peptide. E: Site-specific acetylation rates of K18ac and K23ac of the single-acetylated (1x ac) and double-acetylated (2x ac) H3(18-26) species. n = 3 independent experiments. Statistical analyses were performed using the two-tailed unpaired t-test.